

Article

Ultrashort Laser Texturing of Superelastic NiTi: Effect of Laser Power and Scanning Speed on Surface Morphology, Composition and Wettability

Carlo Alberto Biffi ^{1,*} , Jacopo Fiocchi ¹ , Marzio Rancan ² , Sofia Gambaro ³, Francesca Cirisano ³, Lidia Armelao ^{4,5} and Ausonio Tuissi ¹

¹ National Research Council, Institute of Condensed Matter Chemistry and Technology for Energy, CNR ICMATE Unit of Lecco, Via Previati 1E, 23900 Lecco, Italy

² National Research Council, Institute of Condensed Matter Chemistry and Technology for Energy, CNR ICMATE, c/o Department of Chemistry, University of Padova, Via F. Marzolo 1, 35131 Padova, Italy

³ National Research Council, Institute of Condensed Matter Chemistry and Technology for Energy, CNR ICMATE, Via de Marini, 6, 16149 Genova, Italy

⁴ Department of Chemical Sciences, University of Padova, Via F. Marzolo 1, 35131 Padova, Italy

⁵ Department of Chemical Sciences and Materials Technologies (DSCTM), National Research Council (CNR), Piazzale A. Moro 7, 00185 Roma, Italy

* Correspondence: carloalberto.biffi@cnr.it

Abstract: Among metallic biomaterials, near-equiatomic NiTi is one of the most promising inter-metallic system applicable for biomedical applications, thanks to its high biocompatibility and unique superelasticity (or pseudoelasticity), offering a complete recoverable strain up to 8%. In the prospective uses for bio-devices, the surface processing of NiTi medical components plays a fundamental role for guaranteeing both a Ti oxide passivating layer for avoiding Ni ion release into the human body and surface morphology for controlling the cell proliferation. Mechanical polishing, thermal, chemical or electro-chemical treatments are typically performed for surface modifications. Recently, laser texturing has been successfully applied for different materials, included NiTi shape memory alloys, and also for tuning the surface properties, such as wettability. In the present work, ultrashort laser surface modification was carried out, through the use of a femtosecond laser, for the surface texturing of commercial superelastic NiTi plates. The main goal is to investigate the correlation among morphology, chemical composition and wettability with the principal process parameters, such as average power and scanning velocity in high power ultrashort laser texturing. Laser patterned surfaces were characterized by means of scanning electron microscopy, 3D-profilometry, XPS analysis and wetting measurements. After the laser treatments, both surface morphology and Ni/Ti ratio were largely modified from the initial surface, depending on the adopted process parameters. The wettability of the laser textured surfaces can be also varied with respect to the initial surface, due to the roughness values and grooves induced by the laser beam scans. The laser texturing process induced a combination between micro and nano structures, depending on the input energy. In details, the surfaces were tuned to lower roughness values (from 0.4 μm to 0.3 μm) with a laser power of 1 W, while it was increased up to 0.65 μm with a laser power of 13 W. The laser surface modification promoted a change of the contact angle from 70° of the untreated condition up to 135° to the surface laser treated with a power of 13 W.

Keywords: NiTi; shape memory alloy; laser texturing; femtosecond laser processing; surface modification; XPS; wettability; 3D profilometry



Citation: Biffi, C.A.; Fiocchi, J.; Rancan, M.; Gambaro, S.; Cirisano, F.; Armelao, L.; Tuissi, A. Ultrashort Laser Texturing of Superelastic NiTi: Effect of Laser Power and Scanning Speed on Surface Morphology, Composition and Wettability. *Metals* **2023**, *13*, 381. <https://doi.org/10.3390/met13020381>

Academic Editors: Milan Brandt and Antonio Riveiro

Received: 10 November 2022

Revised: 6 February 2023

Accepted: 8 February 2023

Published: 13 February 2023



Copyright: © 2023 by the authors. Licensee MDPI, Basel, Switzerland. This article is an open access article distributed under the terms and conditions of the Creative Commons Attribution (CC BY) license (<https://creativecommons.org/licenses/by/4.0/>).

1. Introduction

NiTi shape memory alloys (SMAs) are promising smart biomaterials, thanks to their functional properties (shape memory effect—SME, and superelasticity—SE), excellent

corrosion resistance and high biocompatibility [1–4]. However, the high content of Ni (about 50 at%) in biomedical NiTi alloys is a great health issue because the release of Ni ions into the human body can provoke allergic reactions and it may promote carcinogenesis and toxic reactions [5].

It has been shown that the biocompatibility of these materials can be improved through the elimination of Ni from the surface by several surface modification methods [6], such as thermal treatments, plasma immersion ion implantation and deposition as well laser remelting or texturing [7–11]. For instance, an artificial titanium oxide layer can enhance the surface properties and reduce Ni out-diffusion from NiTi. Since NiTi SMA contains a large amount of Ti, it can be readily oxidized to form a titania film by thermal oxidation [12] or by laser induced oxidation [13,14].

On the contrary, laser texturing allows the modification of both the surface topography, due to the material ablation, and the microstructural and/or eventual chemical composition, due to the selective evaporation of single elements [15]. Moreover, these patterns can benefit from the proliferation of osteoblasts on Ti-based alloy surfaces when compared with smooth or acid etched surfaces.

For this reason, in the recent years, ultrashort lasers characterized by pulse durations in the order of femtosecond, have been adopted for precise micro- and nano-machining of several materials, including metals, ceramics and oxides [16]. Compared with short laser pulses, femtosecond lasers can rapidly produce plasma and vapour, thus the surface modification is allowed with limited heat conduction and the consequent formation of a negligible liquid phase [17,18]. Femtosecond laser texturing allows the generation of typical periodic nanostructures, called ripples, under specific process conditions, characterized by high values of energy density, or namely fluence. The dimension of the ripples is around some hundreds of nanometers and they are generated with an orientation perpendicular to the electrical field direction [19,20].

It was found that the laser processing of NiTi SMAs can benefit from the use of ultrashort laser pulses, due to the high sensibility of its microstructure to the heat. The instantaneous vaporization of the material under processing can limit the heat conduction, therefore microstructural modification and compositional change should be minimized. The literature reports relevant results on NiTi surface modifications using low power ultrashort lasers, but nowadays the use of high-power femtosecond lasers need to be deeply investigated on the surface modification area. Therefore, in this work the effect of high power laser texturing of commercial superelastic NiTi plates on the surface morphology, chemical composition and wettability was investigated. The laser textured surfaces were analyzed through SEM, XPS and 3D profilometry, respectively.

2. Experimental Section

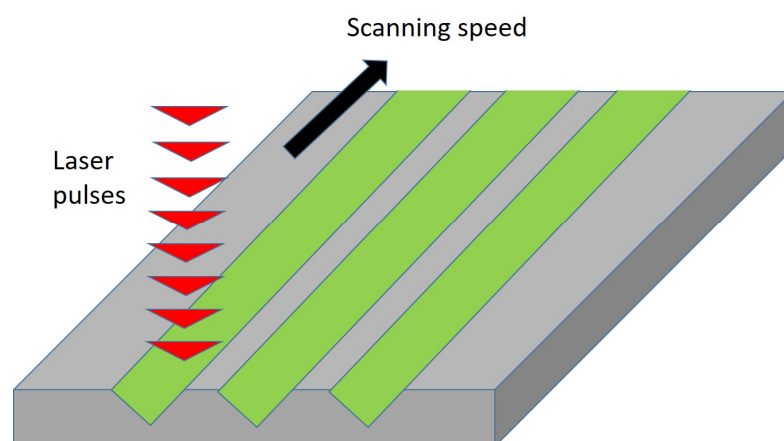
Superelastic Nitinol 250 μm thick plates in straight annealed and electropolished condition were used to be treated by the femtosecond laser for performing texturing experiments. A femtosecond laser (mod. Pharos 15 W from Light Conversion, whose main characteristics are listed in Table 1), coupled with a galvanometer (mod. Cambridge Technology PS1), was used for inducing surface modification on areas of $4 \times 10 \text{ mm}^2$. The experiments were carried out in air by changing laser power and scanning velocity according with a full factorial design of experiments (see the parameters listed in Table 2). The schematic of the laser texturing process is depicted in Figure 1.

Table 1. Main characteristics of the femtosecond laser source used in the texturing experiments.

Characteristic	Values
Maximum average power	15 W
Emission wavelength	1028 nm
Maximum pulse energy	200 μ J
Pulse duration range	210 fs–10 ps
Beam quality factor	1.1
Repetition rate range	Single pulse –200 kHz

Table 2. Variable and fixed process parameters implemented in laser texturing of NiTi tape.

Parameters	Values
Average power	1–13 W
Speed for each pass	2–4 m/s
Pulse duration	213 fs
Laser spot size	18 μ m
Repetition rate	75 kHz
Overlapping	50%

**Figure 1.** Schematic representation of the laser texturing process.

The laser patterned surfaces were analyzed for their morphological characterization using scanning electron microscopy (SEM, mod. Leo 1413).

Surface features and surface roughness (S_a) were quantitatively characterized by the confocal technique using a 3D non-contact profilometer (Sensofar S-neox, Barcelona, Spain) according to the standard ISO 25178, working with 100x objective allowing measurements with a vertical resolution of 1.5 nm (green light was selected). Quantitative measurements were performed using the software embedded in the system (SensoSCAN, Sensofar Metrology, Terrassa, Spain) extracting the surface roughness, S_a ; 5 measurements, done in an area dimension of $130 \times 170 \mu\text{m}^2$, were carried out for defining the variability of each surface [21,22].

XPS analyses were performed with a PerkinElmer Φ 5600-ci spectrometer using Al $K\alpha$ radiation (1486.6 eV), according to a previously described setup [23,24]. Samples were mounted on a steel holder and introduced directly in the fast-entry lock system of the XPS analytical chamber. The XPS spectrometer was calibrated by assuming the BE of the Au $4f_{7/2}$ line at 83.9 eV with respect to the Fermi level. The BE shifts were corrected by assigning to the C 1s peak associated with adventitious hydrocarbons a value of 284.8 eV. The standard deviation for the BEs values was ± 0.2 eV. The sample analysis area was 800 μm in diameter. The

sample analysis area was 800 μm in diameter. Survey scans were obtained in the 0–1350 eV range (187.8 eV pass energy, 0.8 eV step^{-1} , 0.05 s step^{-1}). Detailed scans were recorded for the C 1s, O 1s, Ti 2p and Ni 2p (23.5 eV pass energy, 0.1 eV step^{-1} , 0.1 s step^{-1}). Data analysis involved Shirley-type background subtraction, nonlinear least-squares curve fitting adopting Gaussian–Lorentzian peak shapes, and peak area determination by integration. The atomic compositions were evaluated from peak areas using sensitivity factors supplied by PerkinElmer, taking into account the geometric configuration of the apparatus.

To evaluate the wetting properties of the surfaces, static contact angle (CA) measurements were carried out at room temperature using the ASTRA view tensiometer developed at CNR-ICMATE [25]. High purity grade water, produced by a MilliQ (Milli-Pore, Burlington, MA, USA) ion-exchange purifier with a microfiltration stage, was adopted during the tests. Three replicas were carried out for each surface. Droplets of about 5 mm^3 in volume were gently deposited on the substrate using a microsyringe (Hamilton) with stainless steel capillary of 0.21 mm in diameter. The measurements of CAH were performed changing at low speed (0.1 $\mu\text{L/s}$) the volume of the static drop deposited on the surface.

3. Analysis of Results and Discussion

In Figure 2, 3D-topography as well as 2D profiles of the surfaces, laser patterned at different values of laser power (1 and 13 W) and scanning velocity (2 and 4 m/s) as well as the initial surface, are shown, respectively. Similarly, SEM images of the surfaces, acquired at low and high magnifications for analyzing local modifications induced by the laser beam, are depicted in Figures 3 and 4. As a term of comparison, Figure 5 shows the low and high magnification pictures of the untreated surface.

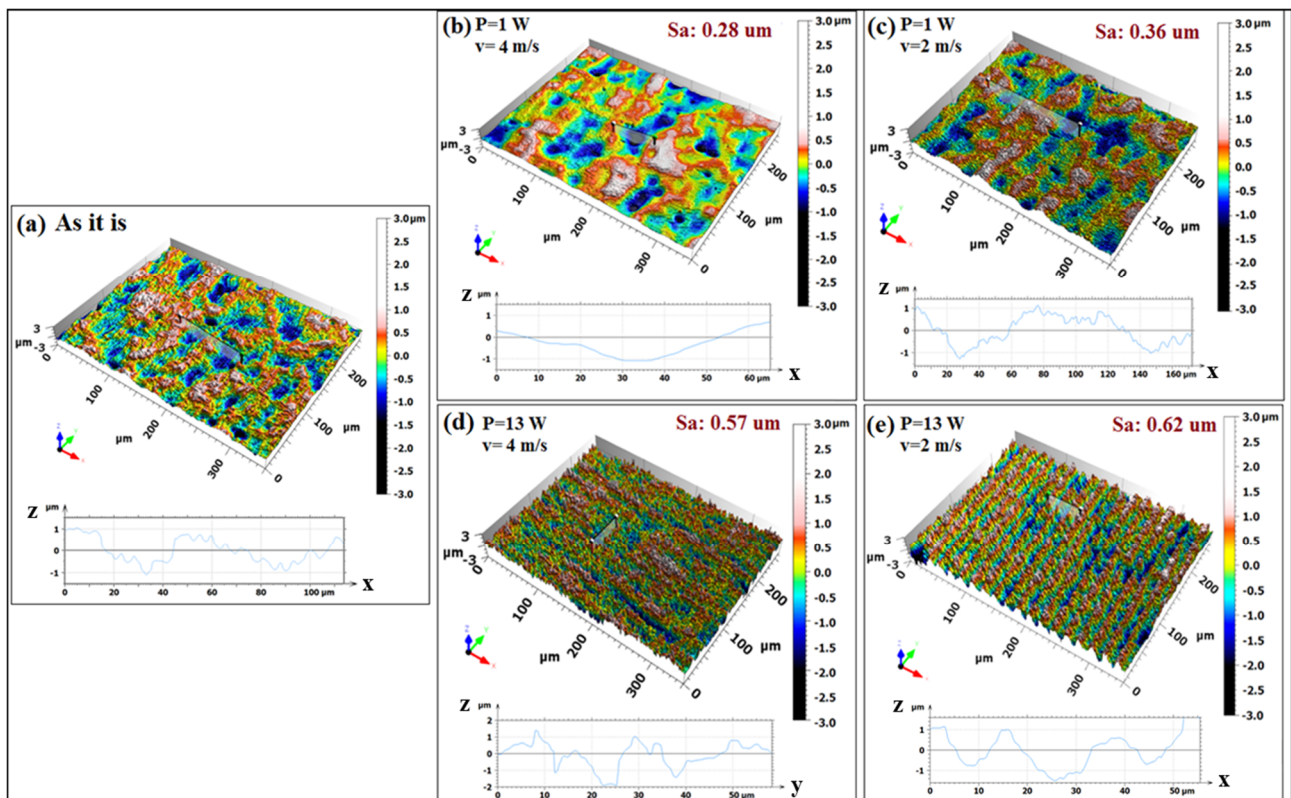


Figure 2. Three-Dimension-profilometry and 2D profile of as it is sample (a); $P = 1\text{ W}$, $v = 4\text{ m/s}$ (b); $P = 1\text{ W}$, $v = 2\text{ m/s}$ (c); $P = 13\text{ W}$, $v = 4\text{ m/s}$ (d) and $P = 13\text{ W}$, $v = 2\text{ m/s}$ (e).

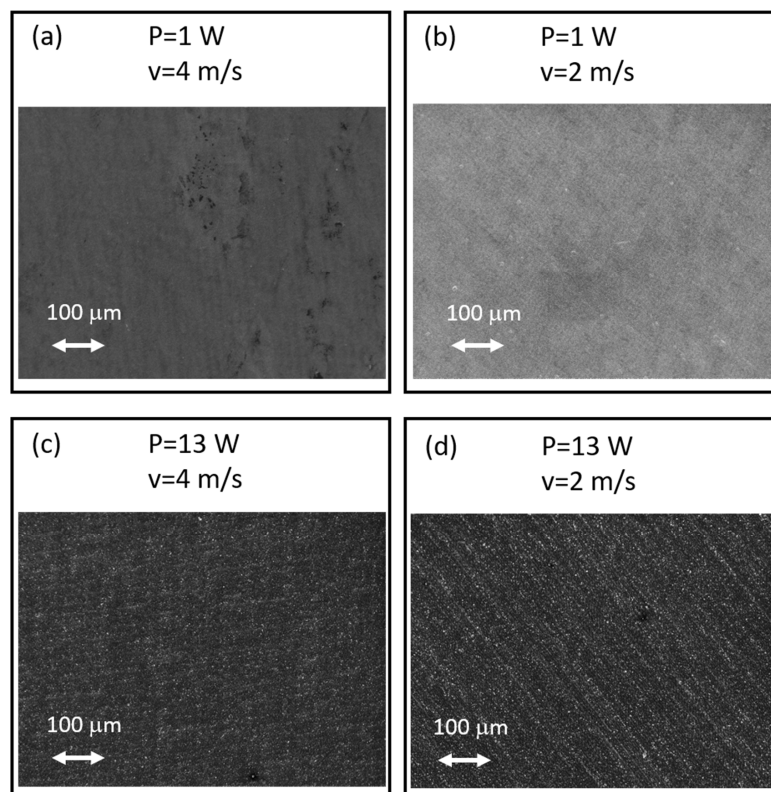


Figure 3. SEM images of the laser textured surfaces, processed at $P = 1\text{ W}$, $v = 4\text{ m/s}$ (a); $P = 1\text{ W}$, $v = 2\text{ m/s}$ (b); $P = 13\text{ W}$, $v = 4\text{ m/s}$ (c); and $P = 13\text{ W}$, $v = 2\text{ m/s}$ (d). SEM images were acquired at low magnification ($500\times$).

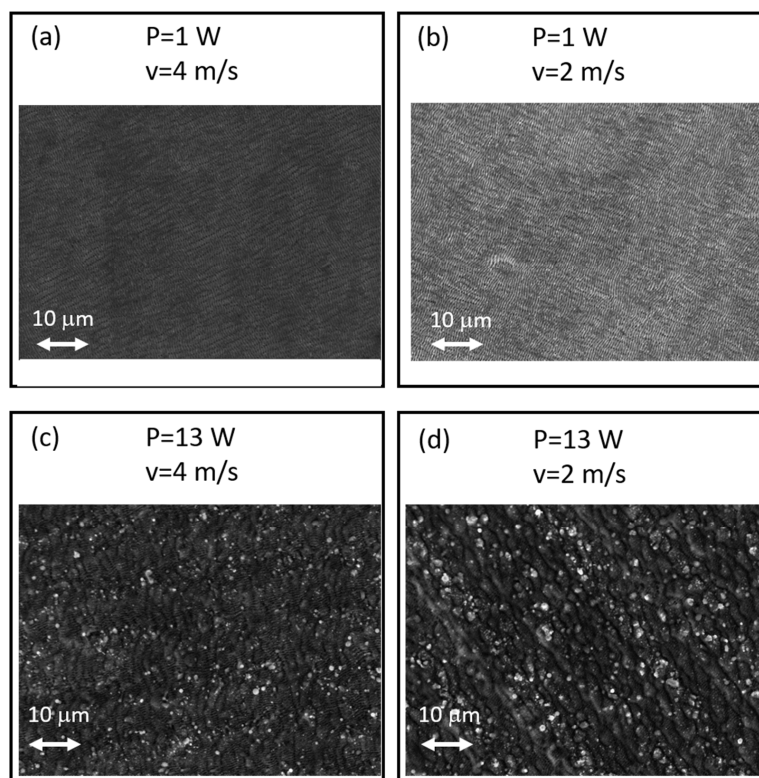


Figure 4. SEM images of the laser textured surfaces, processed at $P = 1\text{ W}$, $v = 4\text{ m/s}$ (a); $P = 1\text{ W}$, $v = 2\text{ m/s}$ (b); $P = 13\text{ W}$, $v = 4\text{ m/s}$ (c); and $P = 13\text{ W}$, $v = 2\text{ m/s}$ (d). SEM images were acquired at high magnification ($3000\times$).

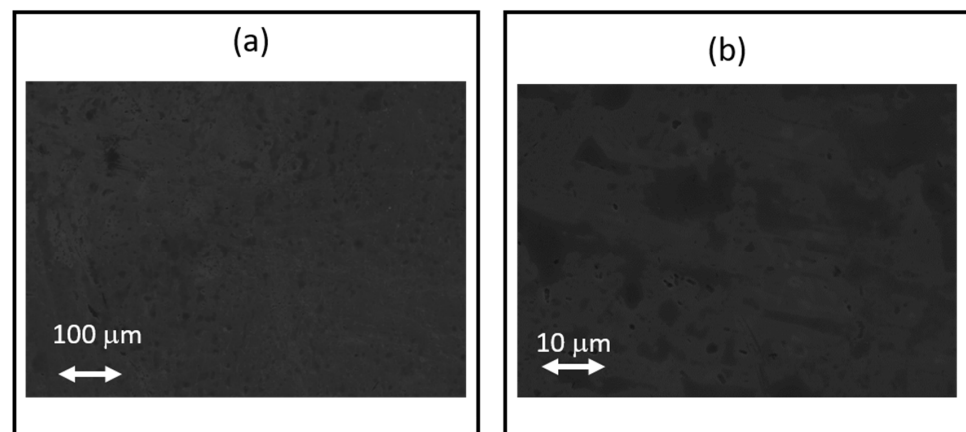


Figure 5. Low and high magnification SEM images of as received sample (a,b).

It can be observed that all the laser textured surfaces exhibited different types of morphology, depending on the adopted process parameters. In details, the morphology of the laser textured surfaces can be modified by using different values of pulse energy E , which can be calculated as follows:

$$E = \frac{P}{v}$$

where P and v represent the laser power and the scanning speed, respectively.

At low magnification, as shown in Figure 2a, the untreated NiTi surface (here referred to as received condition) exhibited the typical morphology of electropolished surfaces, in which some craters are present and it was free from sharp peaks but a smooth surface is evident. Figure 5 shows that no clear nanostructures can be seen, because the material removal in electro-polishing occurs typically in correspondence with the acute angles.

In fact, the laser texturing process, carried out with ultrashort laser pulses (in the range of femtosecond), produced unique features among surface modification methods. The theoretical description indicates that ultrashort laser radiation causes two-photon absorption on the surface. The energy, which is transferred by the photons to the electrons, provokes the vibration of high temperature electrons, therefore the energy is transferred to the surrounding electrons and lattice, increasing the integral temperature of the sample surface [26,27]. When the laser pulse energy reaches the damage threshold value, the lattice of the sample surface starts to break with partial high energy atoms as well as electrons stripping from the surface and splashing away with high velocity. Therefore, plasma can be produced in the laser irradiated zone, due to the direct vaporization of the material or forming bubbles. The shock waves generated during the bubble splitting arouses a transformation in the structure of the sample surface. By increasing the laser power or energy, the bubble size and pressure expanded with the increase in shock depth and width formed by ruptures, thus enlarging the pore size on the sample surface.

During the femtosecond ablation, surface micropatterning can be managed by varying the process parameters. When the sample is irradiated with a low power value (1 W), micropatterns composing ripple-like structures without holes are generated; the orientation of this regular path is perpendicular to the scan direction, as reported in the literature. The size of the ripples is evidently lower than the laser spot size, so their formation cannot be linked to the dimension of the incident beam. As a result, a smooth surface can be obtained using low pulse energy, as seen in Figures 3 and 4, the sub-micrometer surface topography of the laser patterned surfaces under low energy conditions (10 μJ) appear slightly regular with respect to the initial NiTi surface.

Increasing the power up to 13 W (pulse energy of 170 μJ), the modification of the NiTi surface is strengthened and laser induced surface structures can be found to change as well (see Figures 2d–e and 4c–d). A double pattern structure becomes visible: the ripple-like structure is overlapped by a microgroove-like one. This effect of the pulse energy can be

confirmed by the literature [8]. The ablation of the material becomes more aggressive and promotes the realization of irregular surfaces, indicating the presence of a micro-scaled textured surface. The results from the surface tomography indicate the formation of a patterned surface that has both higher values of roughness, if processed with increased power. This achieved both a micro- and macro-modification of the initial surface.

The increase in the roughness can be explained by the enhanced laser ablation process [8]. If the process is performed above the threshold, ripples, microgrooves and holes may be produced on the surface. By increasing more and more energy, the surface can be seriously ablated and deep grooves can be induced and ripples can be formed only at the border of the groove due to the local lower energy.

Moreover, sub-micrometric particles are generated on the surfaces machined with high power values (i.e., 13 W for both the scanning velocity values), due to the large amount of material suddenly vaporized by the laser beam, not removed but instantaneously solidified and in situ redeposited [28]. Similar results were also achieved on other metallic samples, such as FeMn tapes, processed under similar process conditions [29].

Another relevant surface characteristic is represented by the wettability. The homogeneity of peaks and valleys distribution was also confirmed by the symmetry of the droplet for such a sample. Contact angle (CA) images are reported in Figure 6 for all the surfaces. It can be seen that the wetting properties of the different laser textured surfaces are modified, according with the investigated process conditions, when compared with the initial untreated surface.

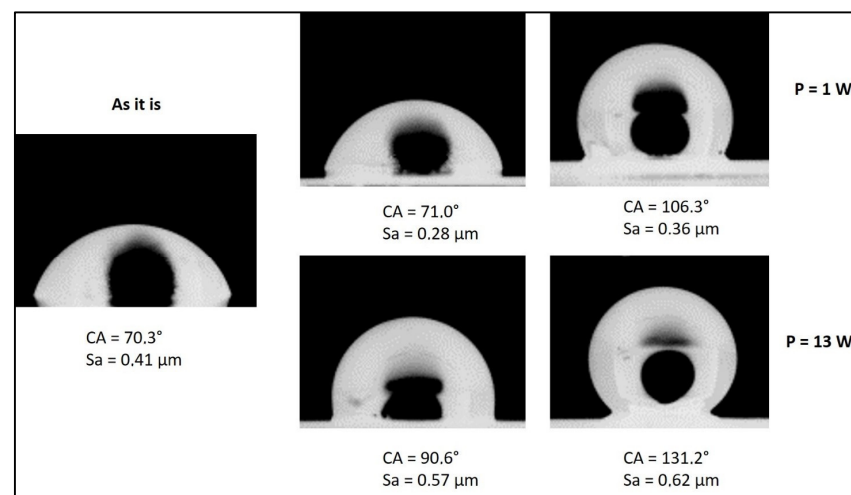


Figure 6. Contact angle of base material (as it is condition) and of samples treated at $P = 1$ W (up) and at $P = 13$ W (down).

Quantitative analysis of the CA and the corresponding roughness (Sa) values of the investigated textured surfaces are shown in Figure 7. The smoothing effect induced by the laser texturing processes, carried out at lower power ($P = 1$ W) on NiTi surfaces, is supported by the measurements of Sa, the value of which appeared lower than that measured for the base material. On the other hand, samples treated at a higher power ($P = 13$ W) presented a rougher surface compared with the initial surface, due to the higher material removal and due to the presence of evident grooves. The scanning speed increase (from 2 m/s up to 4 m/s) promoted a decrease in the Sa values at 1 W, because of the reduction of the linear energy E from 0.5 J/m down to 0.25 J/m. On the contrary, the use of high laser power (13 W) made this trend not actually observable: the values of Sa are in the same range, probably due to the fact that the energy threshold was achieved. In fact, the linear energy E decreased from 6.5 J/m down to 3.25 J/m upon increasing the scanning speed from 2 m/s up to 4 m/s.

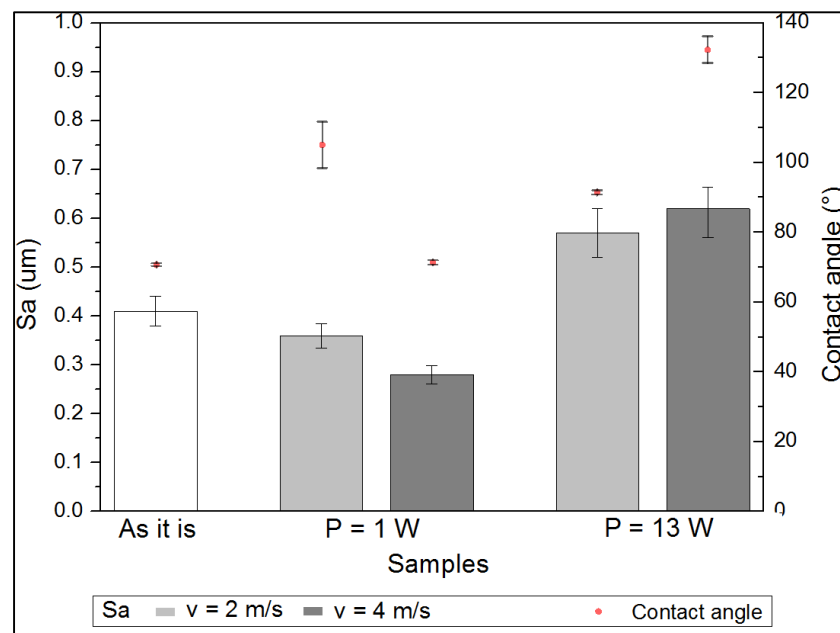


Figure 7. Roughness (Sa) and contact angle values for all tested samples.

In the same graph (see Figure 7) the contact angle values of a high purity water droplet on samples surface are reported. The CA values grow with the increasing of the roughness both for $P = 1$ W and $P = 13$ W samples. Observing the 2D-profiles of samples reported below each 3D-topography (see Figure 2), it is possible to affirm that surfaces treated at $P = 13$ W, $v = 2$ m/s showed the most regular and homogenous pattern.

By changing the process conditions, the CA values were only increased with respect to the untreated surface; this is in good agreement with the literature. In fact, in a previous paper it was found that the CA can be tuned in accordance with the topography induced by the laser texturing process [30]. In detail, if only nanostructures can be generated on the surface, the CA can be decreased with respect to the polished or untreated surface. On the contrary, if a mix of nano and micro-structures can be achieved, such as was detected in the present study, the CA can increase and produce a surface with lower wettability.

XPS analyses were performed on the pristine sample (as it is) and the four laser textured samples to investigate the composition and chemical–physical features of the surface. All samples, including the laser textured surfaces and the initial surface, show similar spectra, as depicted in Figure 8. Particular focus was added to the Ni2p, O1s, Ti2p and C1s regions of the XPS spectrum.

Figure 9a shows survey scans for the untreated and the four processed samples. Due to the similarities of the acquired spectra, only the sample processed with the process parameters ($P = 1$ W, $v = 4$ m/s) are here discussed in detail. Detailed spectra for the other samples are reported in the Supplementary Material section (Figures S1–S4). Figure 9b–d displays the high-resolution scans for the O1s, Ti2p and Ni2p regions. Table 3 reports the binding energies for the O1s, Ti2p and Ni2p photoemission peaks; all the samples have very similar values. The binding energies of the Ti2p and Ni2p peaks suggest that these two elements are present in an oxidized form on the surface. Indeed, the BE of Ti2p is compatible with the presence of Ti^{4+} in an oxide environment [31] and that of Ni2p with the presence of Ni^{2+} in $Ni(OH)_2$ with the characteristic satellite peaks [32,33]. In agreement with this, the photoemission peak of O1s presents two contributions attributable to an oxide (ca. 530 eV) and a hydroxide (ca. 531.5 eV) component, respectively. Table 4 reports the element atomic percentage for the analyzed samples. The variable amount of carbon essentially derives from adventitious carbon. It is worth noting that in the pristine sample the amount of Ni on the surface is significantly lower and its contribution increases at the

increasing of the treatment power (see Ni/Ti ratio in Table 4). The ratio between the two oxygen components remains almost constant.

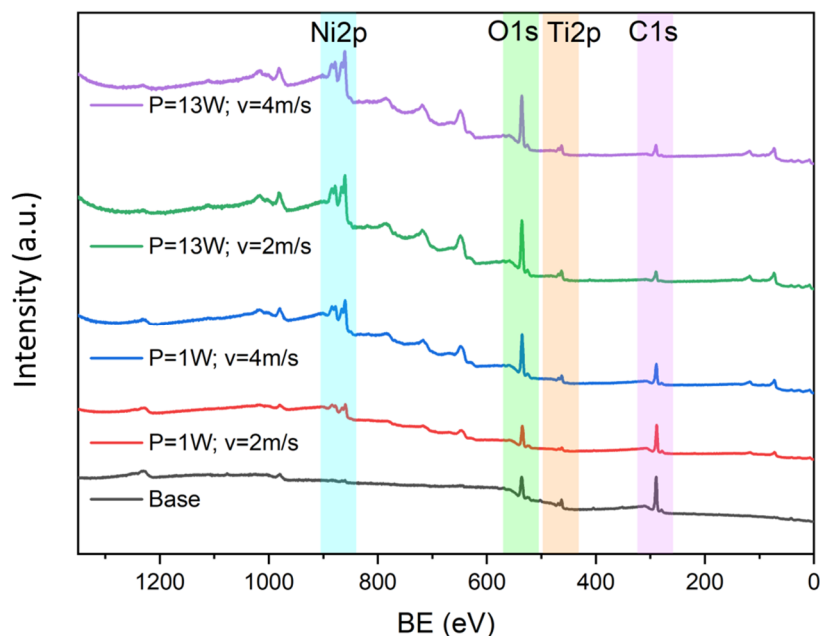


Figure 8. Overview of XPS spectra of the laser textured surfaces and the initial surface (as it is).

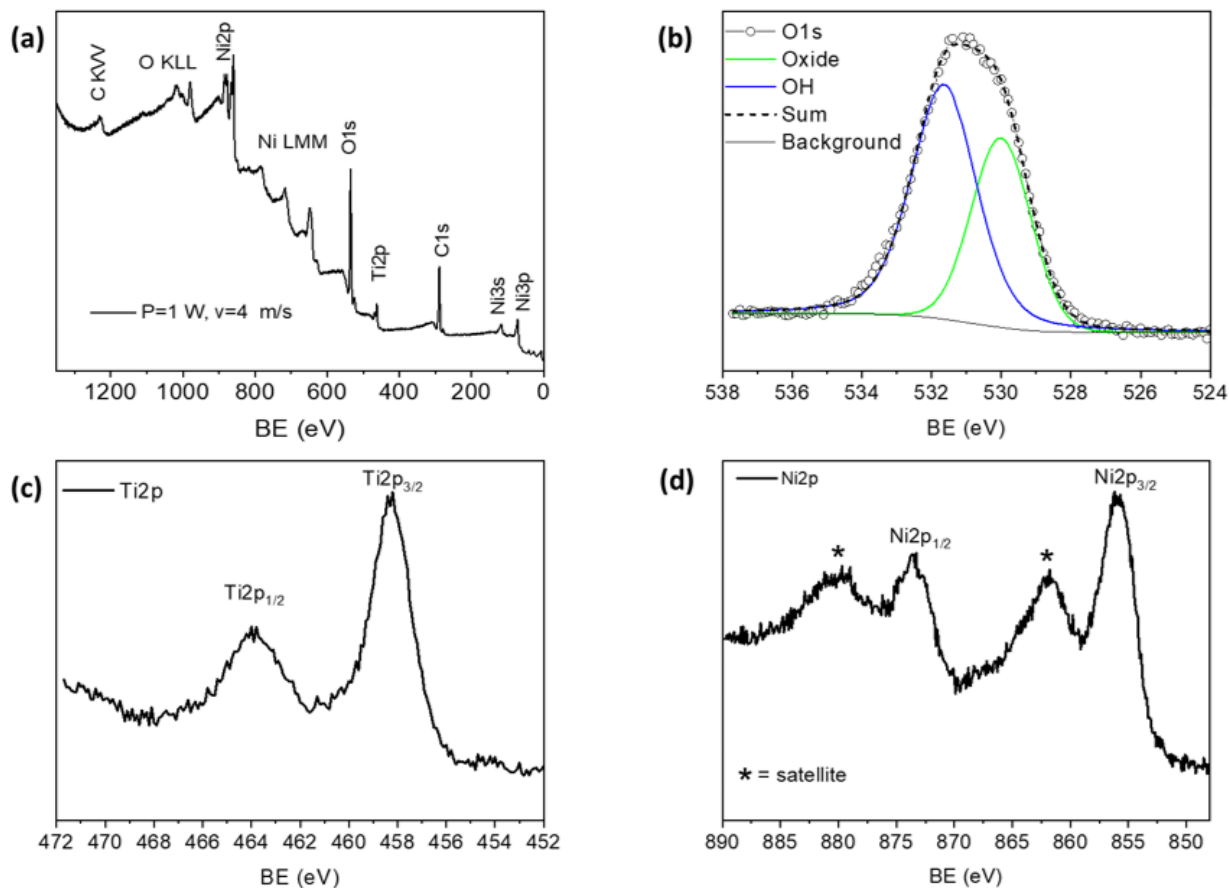


Figure 9. Representative XPS survey (a) and detailed scans (b–d) for the sample $P = 1 \text{ W}$, $v = 4 \text{ m/s}$.

Table 3. Binding energies (eV) O1s, Ti2p and Ni2p regions. O1s photoemission peaks fitted with two components oxide (O_{Ox}) and hydroxide (O_{OH}).

	E [J/m]	O _{Ox}	O _{OH}	Ti 2p _{3/2}	Ni 2p _{3/2}
Base material	-	530.1	531.6	458.1	856.0
<i>P = 1 W, v = 4 m/s</i>	0.25	530.0	531.6	458.2	855.8
<i>P = 1 W, v = 2 m/s</i>	0.5	530.1	531.5	458.5	856.0
<i>P = 13 W, v = 4 m/s</i>	3.25	529.8	531.4	458.2	855.7
<i>P = 13 W, v = 2 m/s</i>	6.5	529.9	531.5	458.1	855.7

Table 4. Atomic percentage for C, O, Ti and Ni elements and Ni/Ti and OH/Ox ratio.

	E [J/m]	C (%)	O (%)	Ti (%)	Ni (%)	Ni/Ti	OH/Ox
Base material	-	72.3	22.7 (Tot) 14.2 (Ox) 8.6 (OH)	3.5	1.5	0.4	1.7
<i>P = 1 W, v = 4 m/s</i>	0.25	43.5	37.7 (Tot) 22.9 (Ox) 17.7 (OH)	3.0	15.8	5.3	1.6
<i>P = 1 W, v = 2 m/s</i>	0.5	65.3	24.6 (Tot) 16.1 (Ox) 8.4 (OH)	1.7	8.4	4.9	1.9
<i>P = 13 W, v = 4 m/s</i>	3.25	24.9	48.1 (Tot) 30.4 (Ox) 17.7 (OH)	3.5	23.5	6.8	1.7
<i>P = 13 W, v = 2 m/s</i>	6.5	22.2	49.1 (Tot) 30.5 (Ox) 18.6 (OH)	3.5	25.2	7.3	1.6

When the energy per unit of length, E, increased, the Ni content on the treated surfaces increased largely with respect to the untreated surface. In fact, the Ni/Ti ratio, in atomic percentage, grew up from 0.4 up to 7.3 upon the increase in energy E. In a previous work, it was found that a limited increase in the Ni/Ti ratio from 0.35 up to 0.82 under an irradiation with lower energy values was detected [8]. Similar results were also achieved in another work, in which femtosecond laser textured surfaces were characterized by an increase in the Ni content on the surface from 0.2 up to 1.58 with respect to the Ti content [30].

4. Conclusions

In the present work, the effect of laser power and scanning speed in surface texturing of superelastic NiTi tapes, carried out using a high-power femtosecond laser, on the morphology, wettability and surface composition was investigated. In detail, the exploration of the investigated process parameters allowed to achieve a correlation with the evaluated surface features of the laser textured areas.

The following was found:

- Varying both laser power and scanning speed allows for the tuning of the average roughness, S_a; in detail, S_a can be decreased from the initial value (0.41 μm) down to 0.28 μm or increased up to 0.62 μm;
- In all the investigated process conditions, a mix of nano- and micro-structures can be achieved;
- The contact angle of the laser-textured surfaces was varied according to the irradiated energy: at the lowest energy, no change with respect to the untreated surface was induced (CA around 70°) while by increasing the energy the contact angle was increased up to 131°, reducing the wettability of the laser textured surfaces;

- The surface Ni/Ti ratio, expressed in atomic percentage, was modified under different laser energy; the Ni/Ti ratio increased from 4.9 up to 7.4 when the laser energy increased, starting from 0.4 in the untreated surface.

Supplementary Materials: The following supporting information can be downloaded at: <https://www.mdpi.com/article/10.3390/met13020381/s1>, Figure S1: Representative XPS survey (a) and detailed scans (b–d) for the pristine sample; Figure S2: Representative XPS survey (a) and detailed scans (b–d) for the sample $P = 1$ W, $v = 2$ m/s; Figure S3: Representative XPS survey (a) and detailed scans (b–d) for the sample $P = 13$ W, $v = 4$ m/s; Figure S4: Representative XPS survey (a) and detailed scans (b–d) for the sample $P = 13$ W, $v = 2$ m/s.

Author Contributions: All authors have participated to all the activities regarding the preparation of the paper. All authors have read and agreed to the published version of the manuscript.

Funding: The authors would like to acknowledge Accordo Quadro CNR/Regione Lombardia n. 3866 FHfFC for their financial support.

Institutional Review Board Statement: Not applicable.

Informed Consent Statement: Not applicable.

Data Availability Statement: The data presented in this study are available on request from the corresponding authors.

Acknowledgments: The authors wish to thank G. Carcano for their support in the experiments and G. D’Amelio from Optoprim srl-Italy for the support in femtosecond laser texturing experiments.

Conflicts of Interest: The authors declare no conflict of interest.

References

1. Duerig, T.; Pelton, A.; Stöckel, D. An overview of nitinol medical applications. *Mater. Sci. Eng. A* **1999**, *273–275*, 149–160. [[CrossRef](#)]
2. Otsuka, K.; Wayman, C.M. *Shape Memory Materials*; Cambridge University Press: Cambridge, UK, 1998.
3. Ming, L.; Jun, L.; Yanxiao, Z. Recent Advances in corrosion research of biomedical NiTi shape memory alloy. *Rare Met. Mater. Eng.* **2021**, *50*, 4165–4173.
4. Wang, J.; Wang, T.; Dong, S.; Kang, X.; Zhao, S.; Shi, H.; Gao, B.; Ma, S.; Liu, M.; Niu, L.; et al. The effect of Cu-doping on the corrosion behavior of NiTi alloy arch wires under simulated clinical conditions. *Mater. Res. Express* **2021**, *8*, 016537. [[CrossRef](#)]
5. Williams, D.F. Toxicology of Implanted Metals. In *Fundamental Aspects of Biocompatibility*; CRC Series in Biocompatibility; CRC Press: Boca Raton, FL, USA, 1981; Volume 2, p. 45. [[CrossRef](#)]
6. Shabalovskaya, S.; Anderegg, J.; Van Humbeeck, J. Critical overview of Nitinol surfaces and their modifications for medical applications. *Acta Biomater.* **2008**, *4*, 447–467. [[CrossRef](#)] [[PubMed](#)]
7. Chu, C.L.; Wang, R.M.; Hu, T.; Yin, L.H.; Pu, Y.P.; Lin, P.H.; Dong, Y.S.; Guo, C.; Chung, C.; Yeung, K.W.K.; et al. XPS and biocompatibility studies of titania film on anodized NiTi shape memory alloy. *J. Mater. Sci. Mater. Med.* **2009**, *20*, 223–228. [[CrossRef](#)]
8. Liang, C.; Wang, H.; Yang, J.; Li, B.; Yang, Y.; Li, H. Biocompatibility of the micro-patterned NiTi surface produced by femtosecond laser. *Appl. Surf. Sci.* **2012**, *261*, 337–342. [[CrossRef](#)]
9. Tian, Y.L.; Zhao, Y.C.; Yang, C.J.; Wang, F.J.; Liu, X.P.; Jing, X.B. Fabrication of bio-inspired nitinol alloy surface with tunable anisotropic wetting and high adhesive ability. *J. Colloid Interface Sci.* **2018**, *527*, 328–338. [[CrossRef](#)]
10. Zhang, D.; Wang, M.; Zhao, Y.; Yang, C.; Yang, Z. Modification of Wettability Property of NITI Alloy by Laser Texturing and Carbon Ion Implantation. In Proceedings of the 2019 IEEE International Conference on Manipulation, Manufacturing and Measurement on the Nanoscale (3M-NANO), Zhenjiang, China, 4–8 August 2019; pp. 224–227. [[CrossRef](#)]
11. Cui, Z.; Li, S.; Zhou, J.; Ma, Z.; Zhang, W.; Li, Y.; Dong, P. Surface analysis and electrochemical characterization on micro-patterns of biomedical Nitinol after nanosecond laser irradiating. *Surf. Coat. Technol.* **2020**, *391*, 125730. [[CrossRef](#)]
12. Chu, C.; Wu, S.; Yen, Y. Oxidation behavior of equiatomic TiNi alloy in high temperature air environment. *Mater. Sci. Eng. A* **1996**, *216*, 193–200. [[CrossRef](#)]
13. Wong, M.; Cheng, F.; Man, H. Laser oxidation of NiTi for improving corrosion resistance in Hanks’ solution. *Mater. Lett.* **2007**, *61*, 3391–3394. [[CrossRef](#)]
14. Michael, A.; Pequegnat, A.; Wang, J.; Zhou, Y.; Khan, M. Corrosion performance of medical grade NiTi after laser processing. *Surf. Coat. Technol.* **2017**, *324*, 478–485. [[CrossRef](#)]
15. Dadbakhsh, S.; Vrancken, B.; Kruth, J.-P.; Luyten, J.; Van Humbeeck, J. Texture and anisotropy in selective laser melting of NiTi alloy. *Mater. Sci. Eng. A* **2016**, *650*, 225–232. [[CrossRef](#)]

16. Meijer, J.; Du, K.; Gillner, A.; Hoffmann, D.; Kovalenko, V.; Masuzawa, T.; Ostendorf, A.; Poprawe, R.; Schulz, W. Laser Machining by short and ultrashort pulses, state of the art and new opportunities in the age of the photons. *CIRP Ann.* **2002**, *51*, 531–550. [[CrossRef](#)]
17. Chichkov, B.N.; Momma, C.; Nolte, S.; Alvensleben, F.; Tünnermann, A. Femtosecond, picosecond and nanosecond laser ablation of solids. *Appl. Phys. A* **1996**, *63*, 109–115. [[CrossRef](#)]
18. Tsukamoto, M.; Asuka, K.; Nakano, H.; Hashida, M.; Katto, M.; Abe, N.; Fujita, M. Periodic microstructures produced by femtosecond laser irradiation on titanium plate. *Vacuum* **2006**, *80*, 1346–1350. [[CrossRef](#)]
19. Dumas, V.; Guignandon, A.; Vico, L.; Mauclair, C.; Zapata, X.; Linossier, M.T.; Bouleffour, W.; Granier, J.; Peyroche, S.; Dumas, J.-C.; et al. Femtosecond laser nano/micro patterning of titanium influences mesenchymal stem cell adhesion and commitment. *Biomed. Mater.* **2015**, *10*, 055002. [[CrossRef](#)]
20. Yang, Y.; Yang, J.; Liang, C.; Wang, H.; Zhu, X.; Kuang, D.; Yang, Y. Sub-wavelength surface structuring of NiTi alloy by femtosecond laser pulses. *Appl. Phys. A* **2008**, *92*, 635–642. [[CrossRef](#)]
21. Haitjema, H. Uncertainty in measurement of surface topography. *Surf. Topogr. Metrol. Prop.* **2015**, *3*, 035004. [[CrossRef](#)]
22. Giusca, C.L.; Leach, R.K.; Helary, F.; Gutauskas, T.; Nimishakavi, L. Calibration of the scales of areal surface topography-measuring instruments: Part 1. Measurement noise and residual flatness. *Meas. Sci. Technol.* **2012**, *23*, 035008. [[CrossRef](#)]
23. Dell’Amico, D.B.; Bertagnolli, H.; Calderazzo, F.; D’Arienzo, M.; Gross, S.; Labella, L.; Rancan, M.; Scotti, R.; Smarsly, B.M.; Supplit, R.; et al. Nanostructured Copper Oxide on Silica-Zirconia Mixed Oxides by Chemical Implantation. *Chem. A Eur. J.* **2009**, *15*, 4931–4943. [[CrossRef](#)]
24. Pelizzo, M.G.; Corso, A.J.; Tessarolo, E.; Böttger, R.; Hübner, R.; Napolitani, E.; Bazzan, M.; Rancan, M.; Armelao, L.; Jark, W.; et al. Morphological and Functional Modifications of Optical Thin Films for Space Applications Irradiated with Low-Energy Helium Ions. *ACS Appl. Mater. Interfaces* **2018**, *10*, 34781–34791. [[CrossRef](#)] [[PubMed](#)]
25. Liggieri, L.; Passerone, A. An automatic technique for measuring the surface tension of liquid metals. *High Temp. Technol.* **1989**, *7*, 82–86. [[CrossRef](#)]
26. Yang, Y.; Yang, J.; Liang, C.; Wang, H.; Zhu, X.; Zhang, N. Surface microstructuring of Ti plates by femtosecond lasers in liquid ambiances: A new approach to improving biocompatibility. *Opt. Express* **2009**, *17*, 21124–21133. [[CrossRef](#)] [[PubMed](#)]
27. Liang, C.; Zhong, X.; Wang, H.; Li, B.; Cai, Y.; Yang, J.; Yang, Y.; Li, C. Femtosecond laser induced micropatterns and in-situ deposition of Ca/P phase and collagen on Ti surface. *Mater. Chem. Phys.* **2015**, *158*, 115–120. [[CrossRef](#)]
28. Biffi, C.A.; Tuissi, A. Nitinol laser cutting: Microstructure and functional properties of femtosecond and continuous wave laser processing. *Smart Mater. Struct.* **2017**, *26*, 035006. [[CrossRef](#)]
29. Biffi, C.A.; Fiocchi, J.; Bregoli, C.; Gambaro, S.; Copes, F.; Mantovani, D.; Tuissi, A. Ultrashort Laser Texturing for Tuning Surface Morphology and Degradation Behavior of the Biodegradable Fe–20Mn Alloy for Temporary Implants. *Adv. Eng. Mater.* **2022**, *24*, 2101496. [[CrossRef](#)]
30. Nozaki, K.; Shinonaga, T.; Ebe, N.; Horiuchi, N.; Nakamura, M.; Tsutsumi, Y.; Hanawa, T.; Tsukamoto, M.; Yamashita, K.; Nagai, A. Hierarchical periodic micro/nano-structures on nitinol and their influence on oriented endothelialization and anti-thrombosis. *Mater. Sci. Eng. C* **2015**, *57*, 1–6. [[CrossRef](#)] [[PubMed](#)]
31. Battiston, S.; Montagner, F.; Zin, V.; Barison, S.; Fiorese, A.; Gionda, A.; Rancan, M.; Sordello, F.; Minella, M.; Biffi, C.A.; et al. Vacuum Thermal Treatments for Surface Engineering of Selective Laser Melted Ti6Al4V Alloy. *J. Mater. Eng. Perform.* **2021**, *30*, 6874–6880. [[CrossRef](#)]
32. Comisso, N.; Rancan, M.; Armelao, L.; Barison, S.; Cattarin, S.; Guerriero, P.; Mattarozzi, L.; Musiani, M.; Vázquez-Gómez, L.; Verlato, E. Investigation on the oxide-oxide galvanic displacement reactions employed in the preparation of electrocatalytic layers. *Electrochim. Acta* **2020**, *341*, 136056. [[CrossRef](#)]
33. Biesinger, M.C.; Lau, L.W.M.; Gerson, A.R.; Smart, R.S.C. The role of the Auger parameter in XPS studies of nickel metal, halides and oxides. *Phys. Chem. Chem. Phys.* **2012**, *14*, 2434–2442. [[CrossRef](#)]

Disclaimer/Publisher’s Note: The statements, opinions and data contained in all publications are solely those of the individual author(s) and contributor(s) and not of MDPI and/or the editor(s). MDPI and/or the editor(s) disclaim responsibility for any injury to people or property resulting from any ideas, methods, instructions or products referred to in the content.